ACS OMEGA

ACS AUTHORCHOICE

http://pubs.acs.org/journal/acsodf

Article

Magnetism in Mixed Valence, Defect, Cubic Perovskites: $BaIn_{1-x}Fe_xO_{2.5+\delta}$, x = 0.25, 0.50, and 0.75. Local and Average Structures

Antonio D. Lozano-Gorrín, Bradley Wright, Paul A. Dube, Casey A. Marjerrison, Fang Yuan, Graham King, Dominic H. Ryan, Cristina Gonzalez-Silgo, Lachlan M. D. Cranswick, Andrew P. Grosvenor, and John E. Greedan*

Cite This: *ACS Omega* 2021, 6, 6017−6029

Read Online

ACCESS | Metrics & More | Article Recommendations | Supporting Information

ABSTRACT: The series $BaIn_{1-x}Fe_xO_{2.5+\delta}$, x = 0.25, 0.50, and 0.75, has been prepared under air-fired and argon-fired conditions and studied using X-ray diffraction, d.c. and a.c. susceptibility, Mössbauer spectroscopy, neutron diffraction, X-ray near edge absorption spectroscopy (XANES), and X-ray pair distribution (PDF) methods. While $Ba_2In_2O_5$ ($BaInO_{2.5}$) crystallizes in an ordered brownmillerite structure, *Ibm*2, and $Ba_2Fe_2O_5$ ($BaFeO_{2.5}$) crystallizes in a complex monoclinic structure, $P2_1/c$, showing seven Fe^{3+} sites with tetrahedral, square planar, and octahedral environments, all phases studied here crystallize in the cubic perovskite structure, $Pm\bar{3}m$, with long-range disorder on the small cation and oxygen sites. ^{57}Fe Mössbauer studies indicate a mixed valency, Fe^{4+}/Fe^{3+}, for both the air-fired and argon-fired samples. The increased Fe^{3+} content for the argon-fired samples is reflected in increased cubic cell constants and in the increased Mössbauer fraction. It appears that the $Pm\bar{3}m$ phases are only metastable when fired in argon. From a slightly modified percolation theory for a primitive cubic lattice (taking into account the presence of random O atom vacancies), long-range spin order is permitted for the x = 0.50 and 0.75 phases. Instead, the d.c. susceptibility shows only zero-field-cooled (ZFC) and field-cooled (FC) divergences at ∼6 K [5 K] for x = 0.50 and at ∼22 K [21 K] for x = 0.75, with values for the argon-fired samples in [ ]. Neutron diffraction data for the air-fired samples confirm the absence of long-range magnetic order at any studied temperature. For the air-fired x = 0.50, a.c. susceptibility data show a frequency-dependent χ'(max) and spin glass behavior, while for x = 0.75, χ'(max) is invariant with frequency, ruling out either a spin glass or a superparamagnetic ground state. These behaviors are discussed in terms of competing Fe^{3+}−Fe^{3+} antiferromagnetic exchange and ferromagnetic Fe^{3+}−Fe^{4+} exchange. The PDF and ^{57}Fe Mössbauer data indicate a local structure at short interatomic distances, which deviates strongly from the average $Pm\bar{3}m$ model. Fe Mössbauer, PDF, and XANES data show a systematic dependence on x and indicate that the Fe^{3+} sites are largely fourfold-coordinated and Fe^{4+} sites are fivefold- or sixfold-coordinated.

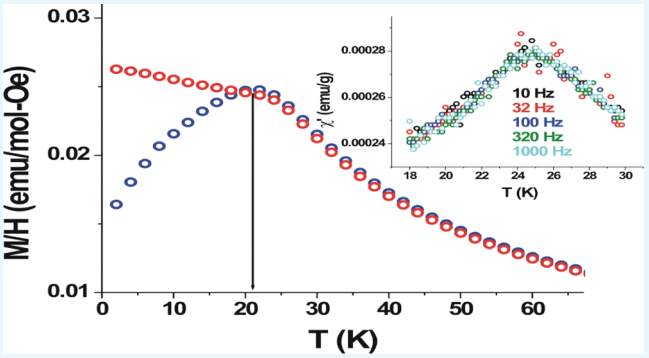

INTRODUCTION

Oxygen deficient perovskite oxides, ABO_{3-x} ($A_2B_2O_5$), comprise a substantial class of perovskite-related materials. There exist two broad structural classes, one in which the O^{2-} vacancies order crystallographically, that is, long-range structural order, and one in which the vacancies appear to be randomly distributed. The most common vacancy-ordered structure is brownmillerite. Here, the vacancies and the B-cations order, resulting in a large supercell with dimensions $a_{bm} \sim \sqrt{2}a_p$, $b \sim 4a_p$, and $c \sim \sqrt{2}a_p$. The structure is characterized by layers of corner-sharing BO_6 octahedra alternating with layers of $B'O_4$ tetrahedral chains. The relationship between the ordered brownmillerite and the parent perovskite structure is illustrated in Figure 1. The crystal class is generally orthorhombic, and the actual space group symmetry is determined by the relative orientation of the $B'O_4$ chains which depends on the precise vacancy ordering pattern within that layer.[1,2] Figure 2 shows the progression from the most to the least degree of vacancy (or O^{2-}) ordering in terms of the space group symmetry. Note that the fully disordered case, $Pm\bar{3}m$, is included. A phase diagram which relates the space group to the chain dipole moment and

Received: January 22, 2021
Accepted: February 8, 2021
Published: February 17, 2021

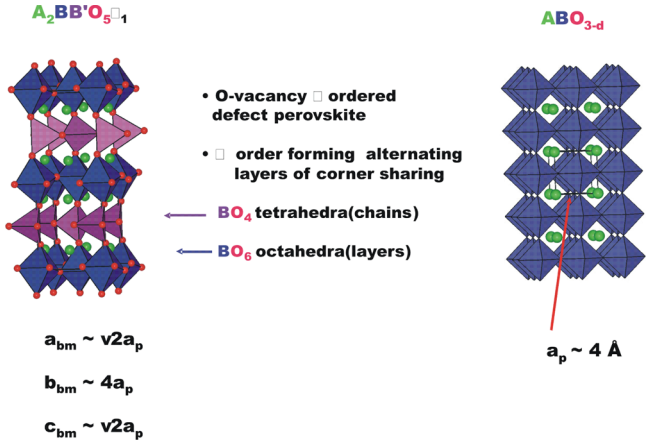

Figure 1. Relationship between the brownmillerite and vacancy-disordered perovskite structures.

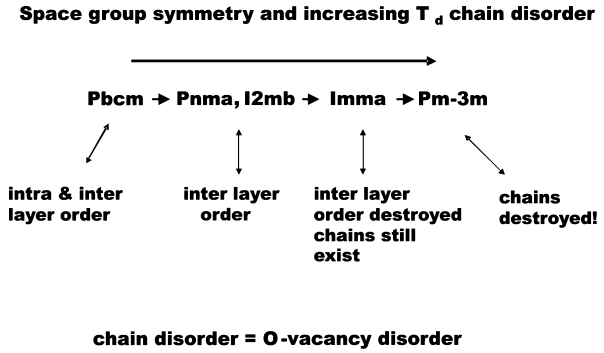

Figure 2. Relationship between the space group and the degree of vacancy disorder in the brownmillerites. The space groups are based on the setting choice $b > c > a$.

interlayer distance, which is accurate with one notable exception, Ca_2FeCoO_5, has been proposed.[3]

An interesting vacancy ordering which deviates from brownmillerite is found for $BaFeO_{2.5}$.[4] In this case, the symmetry is monoclinic, $P2_1/c$, and the vacancy ordering pattern is exceedingly complex, resulting in seven Fe environments, rather than two for brownmillerite.

The presence or absence of vacancy ordering can have a significant impact on physical properties, in particular, magnetism. As many of these materials involve high-spin Fe^{3+}, $S = 5/2$, magnetic spin−spin correlations are of great importance in the easily accessible thermal range 2−400 K. Among the vacancy-ordered phases, the long-range antiferromagnetic magnetic order with $T_N \gg 300$ K is typically found, as indicated in Table 1. The magnetic structure is invariably G-type, that is, all nearest neighbor spin correlations are antiparallel. Dilution of the magnetic sites by substitution of a diamagnetic ion such as Al^{3+} or Ga^{3+} results in a reduction in T_N, but even for a 50% substitution rate, $T_N > 300$ K.[5]

Table 1. Magnetic Ordering Temperatures of Selected Vacancy-Ordered $A_2BB'O_5$ Materials

A	B,B′	S.G.	T_N (K)	ref.
Ca	Fe,Fe	*Pnma*	725	9
Ca	Fe,Mn	*Pnma*	407	10
Ca	Fe,Co	*Pbcm*	580	2
Ca,Sr	Fe,Fe	*I2mb*	>400 K	11
Ca	$Fe_{1.5}$,$Cr_{.5}$	*Pnma*	455	12
Sr	Fe,Fe	*Imma*	693	13
Ba	Fe,Fe	$P2_1/c$	720	4

Among the random vacancy, $Pm\bar{3}m$, phases, magnetic properties are known for a few cases only. The Sr analogue of Ca_2FeMnO_5(*Pnma*), Sr_2FeMnO_5 ($Pm\bar{3}m$), does not show a long-range order but a ZFC/FC divergence at ∼50 K.[6] Neutron diffraction data disclosed broad magnetic reflections consistent with a G-type AF order but with a correlation length of ∼50 Å, that is, nanomagnetism. The bulk susceptibility divergence has been interpreted as a blocking temperature resulting from uncompensated surface spins, that is, superparamagnetism. On the other hand, the Sr analogue of $Ca_2Fe_{1.5}Cr_{.5}O_5$ (*Pnma*), $Sr_2Fe_{1.5}Cr_{.5}O_5$ ($Pm\bar{3}m$), does order with an AF G-type structure at 565 K, more than 100 K higher than the Ca phase![7] An attempt was made to rationalize these surprising results by investigating the local structures of the two $Pm\bar{3}m$ materials with some success. In brief, it was shown that the local structure of $Sr_2Fe_{1.5}Cr_{.5}O_5$ resembled that for a vacancy-ordered brownmillerite, while that for Sr_2FeMnO_5 did not.[8]

It is of course of great interest to investigate additional $ABO_{2.5}$ phases which lead to the system $BaIn_{1-x}Fe_xO_{2.5}$. The structure of $BaFeO_{2.5}$ has already been mentioned, and $BaInO_{2.5}$ ($Ba_2In_2O_5$) crystallizes more conventionally into a brownmillerite structure, *Ib2m* (I2mb in the setting $b > c > a$).[14] In the following, the results of a study of three members of this system, $x = 0.25$, 0.50, and 0.75, are described.

Certain members of this system have been reported previously in the context of a study of oxygen absorption/desorption, in particular, the $x = 0.9$ phase, but no magnetic properties have been reported.[15]

EXPERIMENTAL METHODS

Material Synthesis. Samples were prepared using standard solid-state methods involving intimate mixing of appropriate amounts of $BaCO_3$, In_2O_3, and Fe_2O_3. The mixed powders were pressed into rods or pellets and fired in air, initially. The heating schedule was somewhat different for each x, as described in Table 2 below. In particular, the $x = 0.75$ sample melted when fired above 1250 °C.

Table 2. Air-Firing Conditions for $BaIn_{1-x}Fe_xO_{2.5+\delta}$ Samples

x	T (°C)	duration (h)
0.25	1350	48
0.50	1350, 1250	48, 48
0.75	1250	48

Samples were also prepared by refiring the air-fired samples, described above in argon at 1100 °C for 12 h, and hence referred to as the argon-fired samples.

X-ray Powder Diffraction. Sample purity was checked by X-ray powder diffraction, and a Rietveld refinement was carried out for each sample using data from a PANalytical X'Pert PRO (PANalytical, Almelo, Netherlands) with Cu-Kα_1 radiation (λ = 1.54056 nm) and X'Celerator detector with a 2 theta step of 0.0167°.

X-ray PDF Measurements. Total scattering data were collected at the Brockhouse High Energy Wiggler Beamline of the Canadian Light Source using an X-ray wavelength of 0.1938 Å and a Perkin Elmer area detector. The samples were contained in Kapton capillaries with inner diameters of 0.615 mm. The

https://dx.doi.org/10.1021/acsomega.1c00416
ACS Omega 2021, 6, 6017−6029

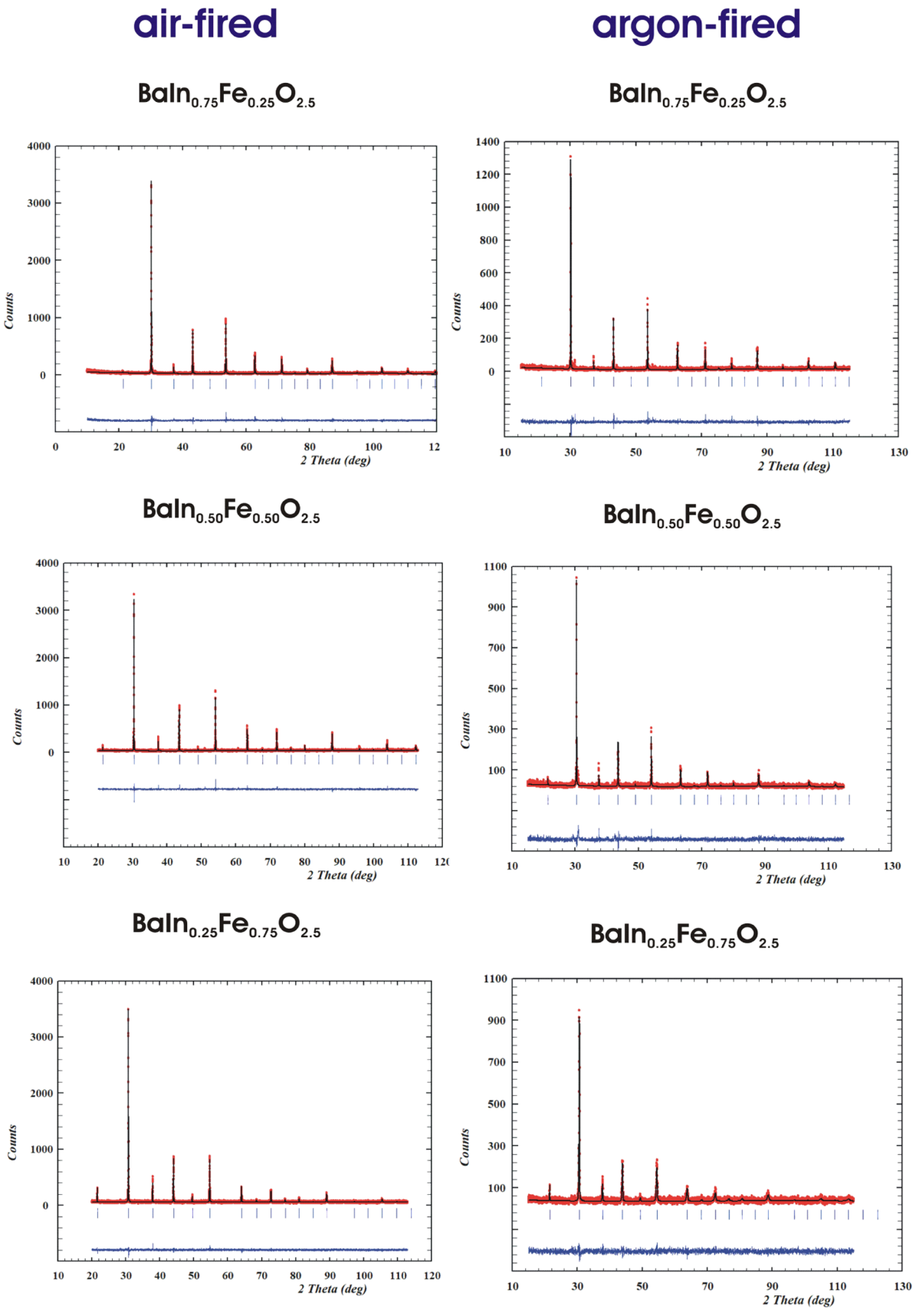

Figure 3. Rietveld refinements for $BaIn_{1-x}Fe_xO_{2.5+\delta}$, x = 0.25, 0.50, and 0.75 for air-fired and argon-fired samples.

data were processed using GSAS-II,[16] and a Q_{max} of 25 Å^{-1} was used to generate the PDFs.

Magnetic Susceptibility. D.c. data were collected using a MPMS SQUID magnetometer from Quantum Design. The

https://dx.doi.org/10.1021/acsomega.1c00416
ACS Omega 2021, 6, 6017−6029

Table 3. Refinement Results for $BaIn_{1-x}Fe_xO_{2.5+\delta}$ Fired in Air[a]

x	a_0 (Å)	B_{Ba} (Å^2)	$B_{In/Fe}$ (Å^2)	B_O (Å^2)	R_{wp} (%)	χ^2
0.25	4.1818(1) [4.1864(2)]	0.85(9) [0.1(2)]	1.3(1) [0.4(2)]	1.9(5) 0.6(4)	20.8 [28.8]	1.51 [1.50]
0.50	4.14772(9) [4.1491(3)]	0.13(8) [0.7(2)]	0.8(1) [1.7(3)]	1.2(4) [3.0(1)]	16.8 [23.7]	1.30 [1.46]
0.75	4.1069(1) [4.1204(5)]	1.17(8) [1.1(1)]	2.2(1) [1.8(2)]	1.2(3) [0.5(4)]	13.5 [16.8]	1.17 [1.20]

[a] $Pm\bar{3}m$. Ba (1a), In/Fe (1b), O (3c) [values for argon-fired samples].

temperature range was typically 2−400 K. Isothermal field sweep measurements were carried out with applied fields to 5 T. A.c. data were measured in the range 2−40 K in temperature steps of 0.2 K and at frequencies of 10, 100, 320, and 1000 Hz with an a.c. amplitude of 3.5×10^{-4} T.

Mössbauer Spectroscopy. The Mössbauer spectra were obtained on a conventional constant acceleration spectrometer using a 50mCi ^{57}Co(Rh) source calibrated with an alpha-Fe foil at ambient temperatures. Isomer shifts are quoted relative to the center of the calibration spectrum. The low-temperature data were obtained using a vibration-isolated closed-cycle refrigerator. The paramagnetic components of the spectra were fitted to a sum of Lorentzian lines. However, the x = 0.75 spectra exhibited two broadened magnetic contributions (the second only appearing below 25 K), and these were fitted by assuming a distribution of hyperfine fields. For the component that persisted to 300 K, an asymmetric distribution that was broadened only toward the low field side was used, while a symmetrically broadened Gaussian distribution was used for the component that appeared below 25 K.

Neutron Diffraction. Neutron powder diffraction data were collected using the C2 diffractometer operated by the Canadian Neutron Beam Centre at the Chalk River Nuclear Laboratory, Chalk River Canada. The neutron wavelengths are 2.37192 and 1.33052 Å.

XANES. Fe K-edge XANES spectra were collected at the Advanced Photon Source (APS) using the Sector 20 and Sector 9 bending magnet beamline (20-BM; CLS@APS) and a Si (111) crystal monochromator.[17] All spectra were collected using an energy step size of 0.15 eV/step through the absorption edge. Fe metal foil was used as a reference with the absorption edge energy set to 7112 eV for the Fe K-edge XANES spectra.[18] The resolution of the spectra was 0.9 eV at 7112 eV (Fe K-edge). Samples were prepared by spreading a thin layer of finely ground powder between Kapton tape. Spectra were collected in the partial fluorescence yield mode using a 13 element Ge detector or a PIPS detector. All spectra were analyzed using the Athena software program.[19]

RESULTS

Average Crystal Structure. *Air-Fired Samples.* Figure 3 shows Rietveld refinements of powder X-ray diffraction data for the three samples, x = 0.25, 0.50, and 0.75, and the results are shown in Table 3. All samples crystallize in $Pm\bar{3}m$, the cubic, fully disordered structure. To summarize this section, all three series members show an average structure with cubic perovskite symmetry, $Pm\bar{3}m$. The local structures will be discussed in a later section.

Argon-Fired Samples. As will be discussed in a later section, there it is evident that the air-fired samples contain a mixed oxidation state, Fe^{3+}/Fe^{4+}. Thus, attempts were made to prepare samples with Fe^{3+} only or at least to maximize its concentration. Firing the starting materials, $BaCO_3$, Fe_2O_3, and In_2O_3, in argon to prepare the x = 0.50 phase failed. While an initial firing at 1100 °C for 24 h resulted in a $Pm\bar{3}m$ phase with an increased cell constant, a ∼4.158 Å, the peak widths were ∼2 x those for the air-fired sample. A second firing under the same conditions resulted in complete decomposition, Supporting Information Figure 1, into phases yet unidentified but are possibly $Ba_2In_{2-x}Fe_xO_5$ and $BaFe_{1-x}In_xO_{2.5}$. A color change from black to green was noted. It thus appears that $Pm\bar{3}m$ phases containing only Fe^{3+} are metastable at best. A second attempt involved subjecting the air-fired samples just described above to a firing in argon at 1100 °C for 12 h. Under these conditions, complete decomposition was avoided and a $Pm\bar{3}m$ phase resulted with only a small contamination of other phases, Supporting Information Figure 2. The X-ray diffraction results are shown also in Figure 3 and Table 3. It is clear from Table 3 that the argon-fired samples show larger cell constants than the air-fired versions, indicating an increased Fe^{3+} content.

The nonexistence of thermodynamically stable disordered perovskite phases containing only Fe^{3+} renders the determination of the actual oxygen content, that is, δ, using conventional techniques such as thermogravimetric analysis (TGA), highly problematic.

For example, either a simple weight gain experiment by firing an Fe^{3+}-only perovskite phase in air or a weight loss experiment by firing an air-prepared sample in argon to produce an Fe^{3+}-only phase is not possible. It will be shown in a later section that while the argon-fired samples do indeed have a smaller Fe^{4+} content, all such samples remain mixed valence. As will be explained in a later section, the ^{57}Fe Mössbauer results provide an accurate measure of the Fe^{3+}/Fe^{4+} content.

All three air-fired samples and the x = 0.50 and 0.75 argon-fired samples were further investigated by magnetization and Mössbauer spectroscopy as interesting magnetism is possible for these two compositions and not the x = 0.25 phase, as will be argued in a later section. In addition, as mentioned above, Mössbauer spectroscopy can also provide an accurate measure of the Fe valence.

Magnetic Properties. *D.c. Susceptibility.* Bulk magnetization data were collected on five samples, three air-fired and two argon-fired, over the range 2−400 K at an applied field of 100 Oe (10^{-2} T) in both the zero-field-cooled (ZFC) and field-cooled (FC) modes. Isothermal magnetization data were also obtained at various temperatures up to 5 T applied field.

It is important to anticipate what might be expected by assuming that the average structure determines the bulk magnetic properties of these systems. The magnetic lattice is the simple or primitive cubic lattice (s.c.), and the materials can be initially regarded as a series of dilute antiferromagnets. Here, percolation theory would presumably be a reasonable guide and for the s.c. lattice, the site percolation threshold, assuming only near neighbor interactions, is p_c = 0.31.[20] In this case, this value is likely too small because 1/6 of the O^{2-} ions is randomly missing and the number of exchange pathways between n.n. is actually 5 rather than 6, assuming that 180° superexchange is the relevant exchange mechanism. One might estimate a p_c for the five n.n. cases by interpolation between the four n.n. lattices (diamond) of 0.43 and the sixfold lattice, s.c., which would give a

https://dx.doi.org/10.1021/acsomega.1c00416
ACS Omega 2021, 6, 6017−6029

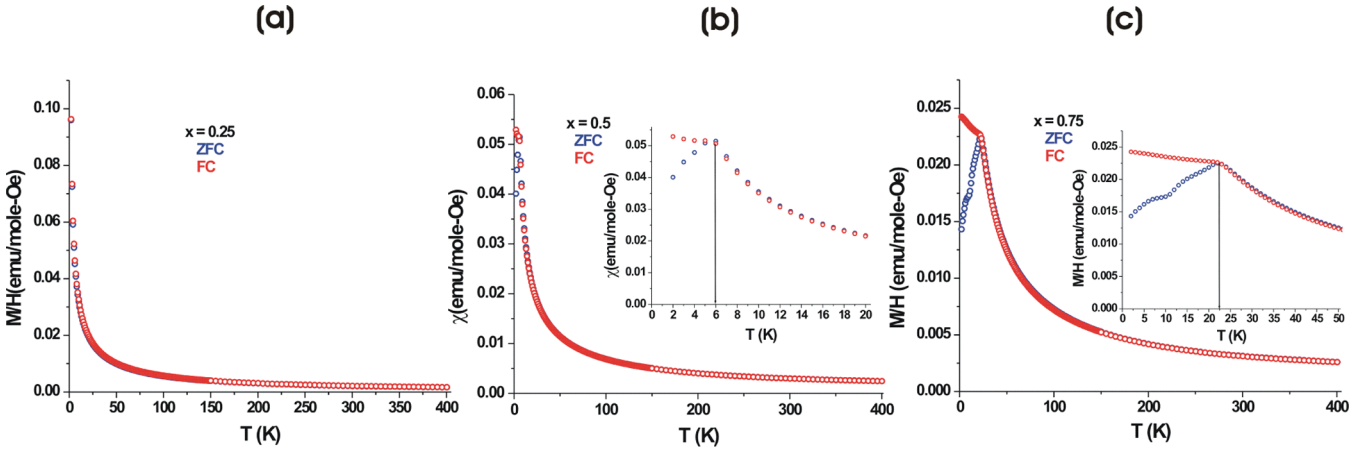

Figure 4. D.c. susceptibility data for air-fired $BaIn_{1-x}Fe_xO_{2.5}$ samples, $x = 0.25$ (a), $x = 0.50$ (b), and $x = 0.75$ (c). The applied field is 10 mT (100 Oe). Note ZFC/FC divergences for $x = 0.50$ at 6 K and 0.75 at 23 K.

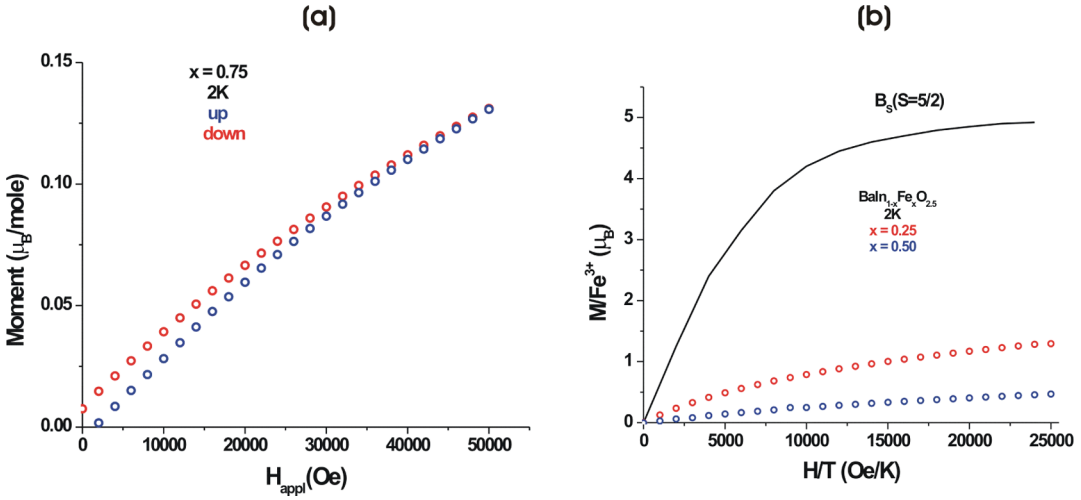

Figure 5. Air-fired samples. (a) First-quadrant hysteresis for $x = 0.75$. (b) Comparison of the field dependence of the Fe^{3+} moment in $x = 0.25$ and 0.50 with the Brillouin function for $S = 5/2$.

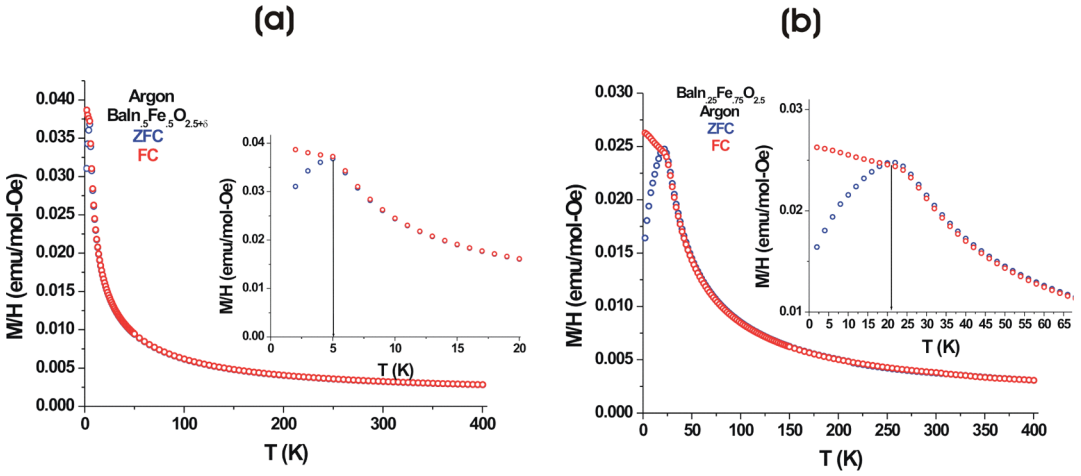

Figure 6. D.c. susceptibility data for the argon-fired samples (a) $Fe_{0.50}$ and (b) $Fe_{0.75}$.

value near 0.37.[20] Thus, at least two members of the series $x = 0.50$ and 0.75 should show a long-range AF order or at least long-range spin correlations with critical temperatures near or exceeding 300 K, according to Table 1.

As the results of Figures 4 and 5 indicate, this is not the case for the air-fired samples nor, Figure 6, for the argon-fired versions. For $x = 0.25$, (6a) the data appear to be consistent with paramagnetism, as might be expected, but for $x = 0.50$ (6b) and 0.75 (6c), ZFC/FC divergences are seen at 6 and 23 K,

https://dx.doi.org/10.1021/acsomega.1c00416
ACS Omega 2021, 6, 6017−6029

respectively, with no sign of the long-range order. Only the x = 0.75 phase shows any hysteresis at 2 K, Figure 5a, and for x = 0.25 and 0.50, comparison with a Brillouin function for S = 5/2, 7b, indicates a strong deviation from simple paramagnetic behavior.

Perhaps surprisingly, for the x = 0.50 and 0.75 argon-fired samples, Figure 6, the low-temperature magnetic behavior is essentially unchanged with ZFC/FC divergences at 5 K (x = 0.50) and 21 K (x = 0.75).

In addition to the results of Figures 4−6, the inverse susceptibility data were examined as indicated in the Supporting Information, Figure 3. It was not always possible to identify a true Curie−Weiss temperature regime for some of the samples. Using only the highest temperature data, 300−400 K, in most cases, a set of Curie−Weiss constants were extracted, Table 4. It is possible that a true C−W regime does not exist within the measured temperature range for most of these materials, so any conclusions should be regarded with some caution. Nonetheless, it is clear that with one exception, the Curie constants are much below the spin-only value for Fe^{3+}, S = 5/2, of 4.38, although increases are seen in going from air- to argon-fired samples. Note that C for the x = 0.50 argon-fired case is actually very near the expected Fe^{3+} value. It is not immediately clear which Curie constants apply for Fe^{4+}, in the high-spin state ($t_{2g}^3e_g^1$), S = 2 and C = 3.00, while for low spin (t_{2g}^4), S = 1 and C = 1.00.

Table 4. Curie Constants and θ_c from Fits to High-Temperature Susceptibility Data for Both Air- and Argon-Fired Samples of $BaIn_{1-x}Fe_xO_{2.5+\delta}$

x	C/Fe (air)	θ_C (K)	C/Fe (argon)	θ_C (K)
0.25	3.17	−72(3)		
0.50	2.71	−152(2)	4.34(4)	−373(6)
0.75	2.03	−188(4)	2.25(4)	−151(2)

A.c. Susceptibility. Given the appearance of ZFC/FC divergences for the x = 0.50 and 0.75 samples, both air- and argon-fired, there are two possibilities for the magnetic ground state which can be tested via a.c. susceptibility measurements, namely, a spin glass and a superparamagnet. In both cases, one expects a significant shift of the maximum in χ', the real part of the signal.[22] From Figure 7, a shift is seen for the x = 0.50 sample (7a) and upon application of the Mydosh criterion, $\Delta T_f/[T_f(\Delta \log \omega)]$ = 0.0109 with T_f = 5.91 K, spin glass behavior is strongly indicated.[21] Contrastingly, although the data are somewhat noisier, no shift is observed for the x = 0.75 sample (7b) which rules out either a spin glass or a super paramagnetic ground state, a rather surprising result. The same result is found

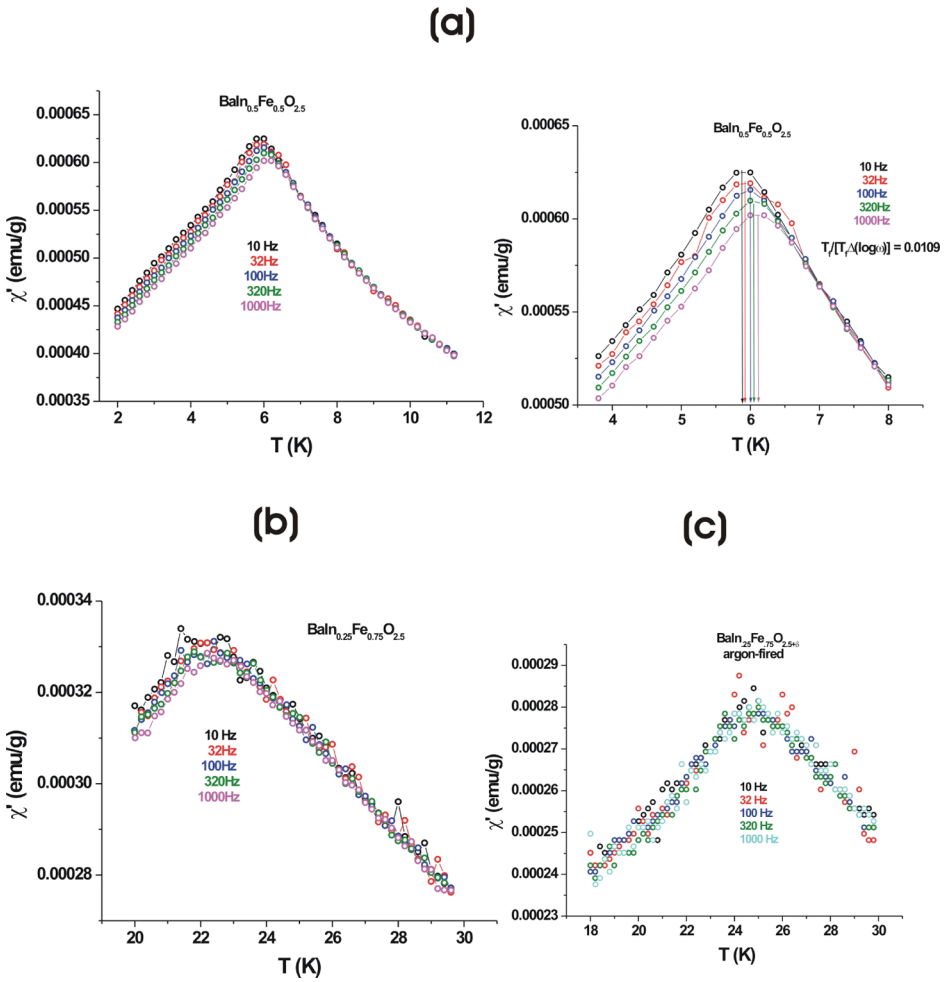

Figure 7. (a) A.c. susceptibility data for air-fired $BaIn_{.50}Fe_{.50}O_{2.5}$, showing a clear frequency shift in χ'(max) and spin glass behavior below T_f = 5.91 K. (b) For air-fired $BaIn_{.25}Fe_{.75}O_{2.5}$, no significant frequency dependence for χ'(max) is evident. (c) Data for the argon-fired $BaIn_{.25}Fe_{.75}O_{2.5}$ sample showing the same behavior.

https://dx.doi.org/10.1021/acsomega.1c00416
ACS Omega 2021, 6, 6017−6029

for the argon-fired $BaIn_{.25}Fe_{.75}O_{2.5}$ sample (7c), although the peak is somewhat sharper and the maximum moves to ~25 K.

Neutron Diffraction. Neutron diffraction data were obtained on the x = 0.75 and 0.50 air-fired samples at 297 and 2.8 K in order to search for magnetic reflections or magnetic scattering of any sort. The results for x = 0.50, Supporting Information Figure 4, show no evidence for magnetic Bragg peaks, assuming a Type G structure with the ordering wave vector $\boldsymbol{k}$ = (1/2 1/2 1/2). For the x = 0.75 sample, there is a very weak feature in the data near the expected position of the (1/2 1/2 1/2) reflection which appears at both temperatures. The width of this peak is roughly twice that of the (100) structural peak. Assuming a magnetic origin, this points to the short-range order at most. Figure 8 shows the results of (a) Rietveld refinement of the 297 K data based only on the crystal structure showing the possible (1/2 1/2 1/2) reflection and (b) a simulation of the crystal and magnetic structures based on an ordered Fe moment of 4.0 μ_B, a typical value for most Fe-based brownmillerites with T_N ~700 K.[9] It is clear that there is no evidence of a true long-range magnetic order for x = 0.50 and 0.75, which show anomalies in the magnetic susceptibility. Short-range magnetic correlations are possible for x = 0.75, even at RT. Assuming a magnetic origin for the indicated peak, an estimate of the Fe moment involved can be obtained by comparison of the intensity of the observed peak with that calculated for a moment of 4.2 μ_B. The intensity ratio is ~1.1%, which implies, taking the square root, a moment of ~0.4 μ_B or ~10% of the full value. One possible interpretation of this result is that there exists a domain representing ~10% by volume of strongly correlated Fe^{3+} ions with moments of ~4 μ_B each, even at RT. Also, as the neutron diffraction patterns for both x = 0.50 and 0.75 show no new features at 2.8 K, Supporting Information Figure 3, there is no magnetic scattering associated with the ZFC/FC divergences. This contrasts with the case of Sr_2FeMnO_5, for which a similar magnetic anomaly was seen at ~50 K and neutron diffraction data at 4 K showed clear evidence for short-range correlations with a domain size of ~50 Å.[6] These features were not observed above 50 K.

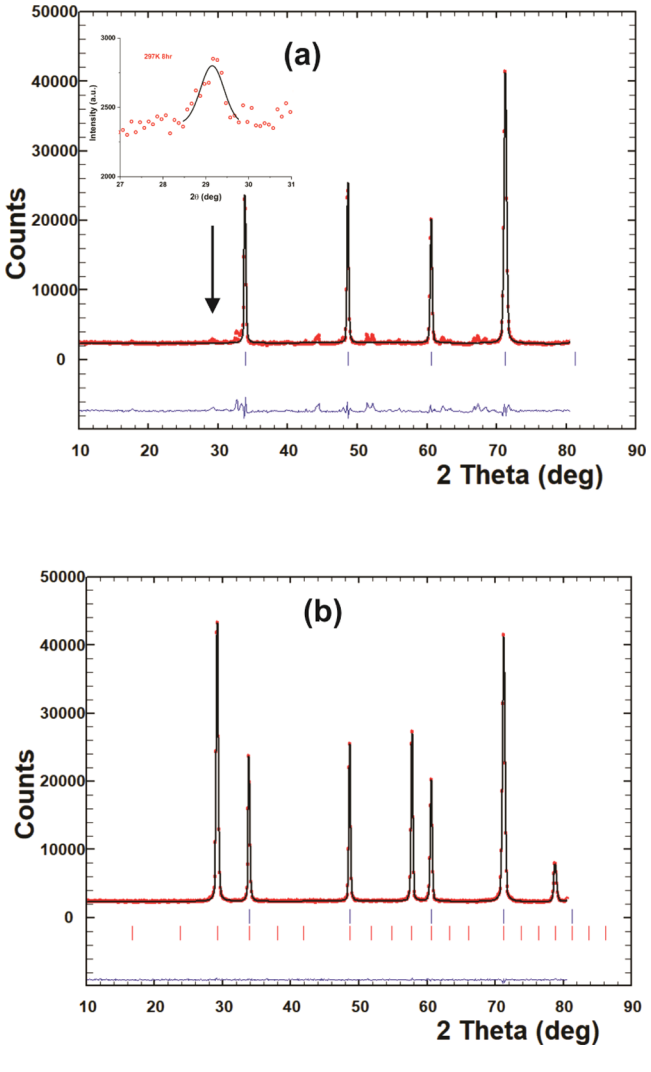

Figure 8. (a) Rietveld refinement of the crystal structure of $BaIn_{0.25}Fe_{0.75}O_{2.5}$ (x = 0.75), showing the presence of a very weak, broad peak (inset) which can be indexed as (1/2 1/2 1/2). (b) Simulation of the crystal and magnetic structures with an ordered Fe moment of 4.0 μ_B. The blue and red tic marks indicate the structural and magnetic peak positions, respectively.

Mössbauer Effect. Mössbauer spectroscopy offers the possibilities to provide a quantitative measure of the Fe^{4+}/Fe^{3+} ratio and to probe the local structure of these materials. Data were obtained for three air-fired and two argon-fired samples at ambient temperature, and for x = 0.75, both air- and argon-fired down to ~10 K. The ambient temperature data are displayed in Figure 9. Data for the air-fired samples could be fit to a two-site model in all cases, while those for the argon-fired samples required a three-site model. The derived isomer shifts (IS), quadrupole splittings (QS), and area fraction A (%) are given in Table 5. For both the air-fired and argon-fired samples, the IS and QS values seem to segregate into two groups, one with a small, often negative, IS with a QS ~0.4 mm/s and one with an IS near ~0.2 mm/s and QS ~1.2 mm/s. Small or negative IS values are associated with Fe^{4+} as found for $SrFeO_{3-y}$,[22] while for the other group, the IS and QS are normally associated with Fe^{3+}, perhaps in fourfold or fivefold coordination. With these assumptions and the observed A (%), one can assign the compositions of the air- and argon-fired samples in terms of the Fe^{3+}/Fe^{4+} content and δ, as shown in Table 6 below.

Thus, the X-ray diffraction data (Table 3), the paramagnetic susceptibility data (Table 4), and the Mössbauer data (Table 6) are all consistent in that the Fe^{3+} content increases upon argon firing, as expected. It is worth noting that in the previous study of an air-fired x = 0.50 sample, a δ = 0.12 value was reported, although the firing conditions were not identical to ours.[15]

These results then allow at least a qualitative understanding of the bulk magnetic properties in terms of competing super-exchange interactions involving high-spin Fe^{3+} ($t_{2g}^3e_g^2$) or ($e_g^2t_{2g}^3$) in either octahedral or tetrahedral sites with either high-spin Fe^{4+} ($t_{2g}^3e_g^1$) or low-spin Fe^{4+}(t_{2g}^4). It seems unlikely that Fe^{4+} in either spin state would occupy a tetrahedral site. By the Goodenough-Kanamori rules, Fe^{3+}–Fe^{3+} exchange would always be antiferromagnetic, while Fe^{3+}–Fe^{4+} interactions would be predominately ferromagnetic, especially for low-spin Fe^{4+},[23] that is, if all Fe were high-spin Fe^{3+} from percolation theory, one would expect a long-range antiferromagnetic order near or above room temperature. However, the presence of significant levels of Fe^{4+} will introduce competing ferromagnetic exchange and states such as a spin glass in the case of x = 0.50 or a more complex disordered state such as that for x = 0.75 can be understood.

Temperature-dependent Mössbauer data were also collected for the air-fired and argon-fired x = 0.75 samples which are shown in Figures 10 and 11, respectively. For the air-fired

https://dx.doi.org/10.1021/acsomega.1c00416
ACS Omega 2021, 6, 6017–6029

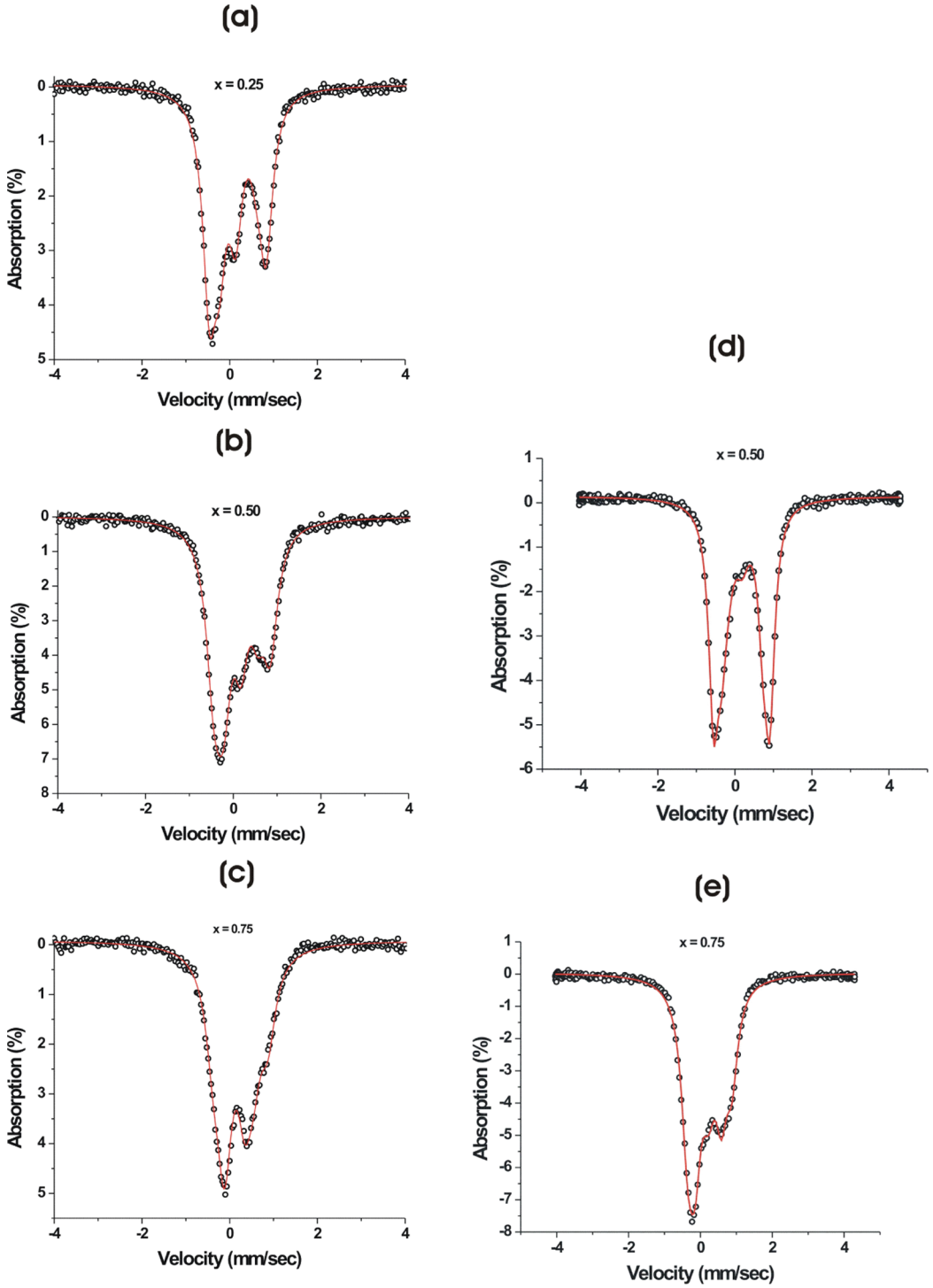

Figure 9. Ambient temperature spectra for the air-fired (a,b,c) and argon-fired (d,e) samples of $BaIn_{1-x}Fe_xO_{2.5+\delta}$. The red lines are fits.

sample, two hyperfine signals are observed. Recall that this phase shows a ZFC/FC divergence at ~23 K and hysteresis at 2 K but no frequency dependence for χ'. Neutron diffraction data were not definitive, but a weak, broad peak which could arise from short range magnetic ordering was observed at RT which was consistent with an ordered Fe moment value of ~10% of that expected. Two magnetic contributions are evident in the spectra of the $x = 0.75$ sample shown in Figure 10a. The first is present at all measured temperatures and grows in area from about 10% at 300 K to about 30% by 11 K (see Figure 10b). This is far too much to be attributed to an impurity phase, and it must therefore be intrinsic to the material. Furthermore, the average hyperfine field (<Bhf>) for this component is almost independent of temperature, increasing from 43 T at 300 K to about 47 T by 11 K, which would imply an ordering temperature well above 300 K. At close to 50 T, the observed hyperfine field is typical of an ordered Fe^{3+} oxide. With caution, this component may be assigned as responsible for the peak observed in the neutron diffraction pattern at RT. However, the reduction in area with increasing temperature indicates that the behavior is more complex than that of a simple long-ranged ordering and more likely reflects some sort of cluster ordering. The second

https://dx.doi.org/10.1021/acsomega.1c00416
ACS Omega 2021, 6, 6017−6029

Table 5. Derived Values for the Isomer Shift (IS), Quadrupole Splitting (QS), and Area Fractions [*A* (%)] for the Air-Fired and Argon-Fired $BaIn_{1-x}Fe_xO_{2.5+\delta}$ Samples

	air-fired				argon-fired			
x	site	IS (mm/s)	QS (mm/s)	*A* (%)	site	IS (mm/s)	QS (mm/s)	*A* (%)
0.25	1	−0.54(5)	0.387(5)	43				
	2	0.171(2)	1.261(4)	57				
0.50	1	−0.014(5)	0.452(9)	46	1	−0.003(9)	0.38(2)	17
	2	0.195(4)	1.175(7)	54	2	0.18(1)	1.458(6)	56
					3	0.191(7)	1.08(1)	27
0.75	1	0.143(3)	0.513(7)	65	1	−0.019(7)	0.49(3)	36
	2	0.285(6)	1.149(1)	35	2	0.25(4)	1.26(1)	29
					3	0.226(3)	0.72(1)	35

Table 6. Fe^{3+} and Fe^{4+} Content and δ for $BaIn_{1-x}Fe_xO_{2.5+\delta}$ Derived from the ^{57}Fe Mössbauer Data with the Assumptions Described in the Text

	air-fired			argon-fired		
x	Fe^{3+}	Fe^{4+}	δ	Fe^{3+}	Fe^{4+}	δ
0.50	0.27	0.23	0.12	0.415	0.085	0.04
0.75	0.26	0.49	0.25	0.48	0.27	0.14

magnetic component only appears below 25 K (Figure 10c), and while <Bhf> is fairly constant at around 20 T once the feature develops, its area grows rapidly on cooling and reaches 50% of the spectral area by 11 K. The onset of a broad magnetic component below 25 K is in good agreement with the maximum in the susceptibility data at 23 K, shown in Figure 8b. As noted earlier, this low-temperature magnetic component is very broad and was fitted using a Gaussian distribution of hyperfine fields that had a width of 10−15 T. The low average value and very broad field distribution indicate that a significant disorder is associated with this magnetic phase, and this disorder may provide part of the explanation for the absence of long-ranged magnetic order despite the iron concentration being well above the percolation threshold for the simple cubic magnetic cell, even if we allow for some reduced connectivity.

The corresponding results for the argon-fired $x = 0.75$, from Figure 11, show only one hyperfine signal with an onset temperature of ∼26 K. The data below ∼26 K were fit to two hyperfine fields, and a weighted average was taken, which is

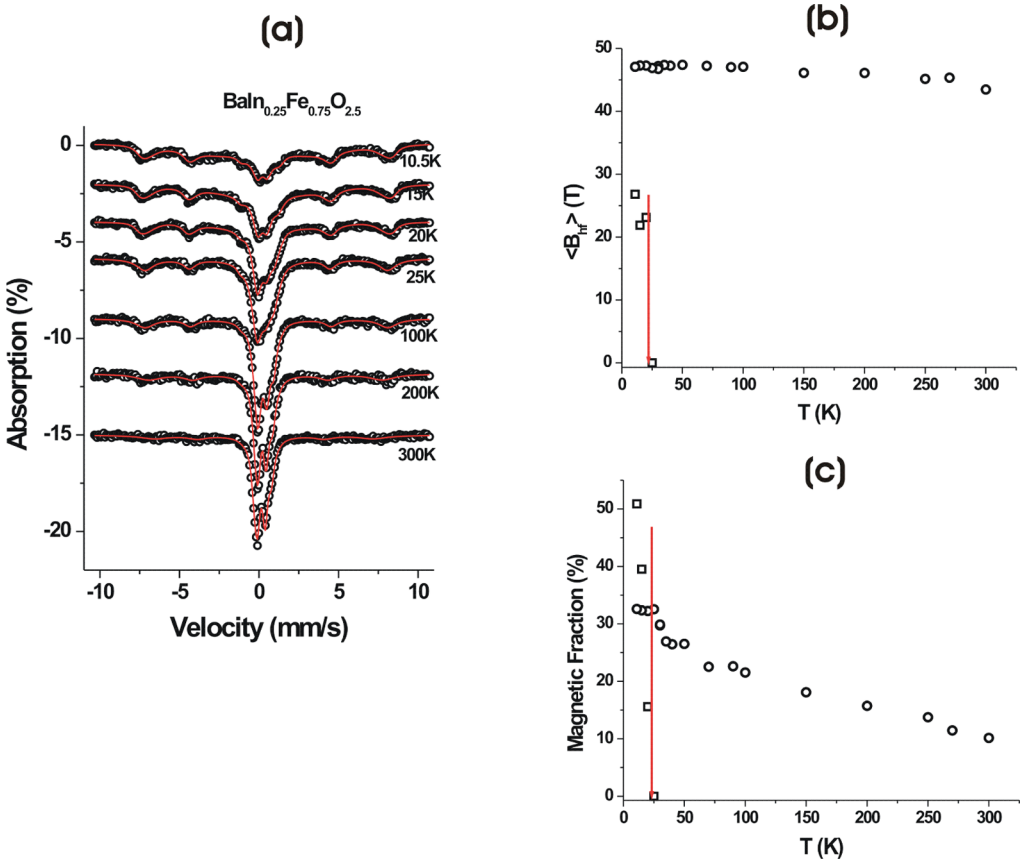

Figure 10. (a) ^{57}Fe Mössbauer spectra for the air-fired $x = 0.75$ sample from 10.5 to 300 K. The red lines are fits. The spectra have been displaced for clarity. (b) Hyperfine field for the high-temperature (circles) and low-temperature (squares) components versus temperature. (c) Hyperfine fraction for both components versus temperature. The red arrows mark the ZFC/FC susceptibility divergence at ∼23 K.

https://dx.doi.org/10.1021/acsomega.1c00416
ACS Omega 2021, 6, 6017−6029

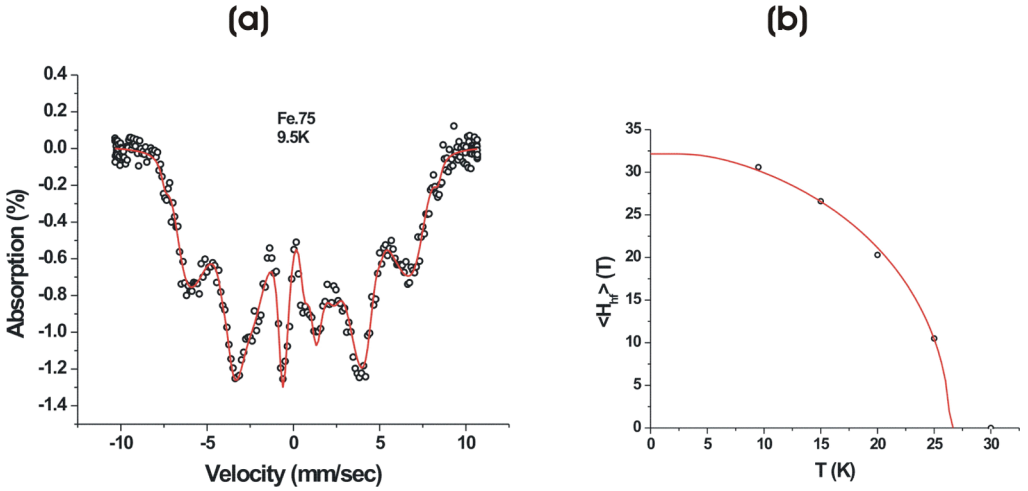

Figure 11. Low-temperature Mössbauer data for argon-fired $BaIn_{.25}Fe_{.75}O_{2.5+\delta}$. (a) Data at 9.5 K showing hyperfine splitting. The red line is a fit to two hyperfine fields. (b) Fit to the temperature dependence of the average H_{hf} vs temperature giving an onset temperature of 26.4(2) K.

shown in Figure 11b. This information is given in Supporting Information, Table 1.

Fe K-Edge XANES. Another technique which can provide information on Fe-oxidation states is X-ray absorption near edge spectroscopy (XANES). Data were collected for all three air-fired samples along with two standards, $LaFeO_3$ (Fe^{3+}) and $SrFeO_3$ (Fe^{4+}), for the Fe K-edge absorption, Figure 12.

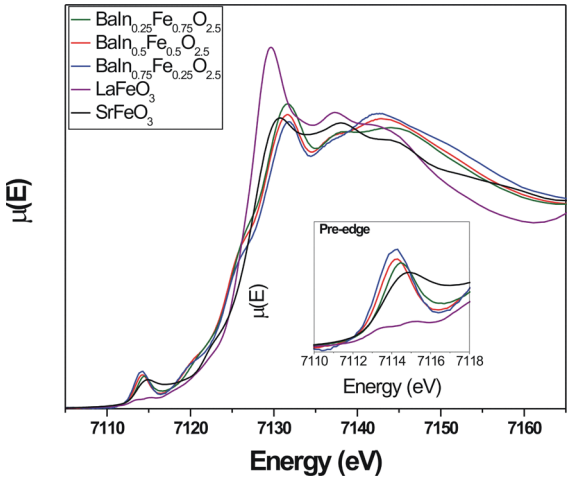

Figure 12. Fe K-edge XANES data for three $BaIn_{1-x}Fe_xO_{2.5+\delta}$ air-fired samples and two standards, $LaFeO_3$ (Fe^{3+}) and $SrFeO_3$ (Fe^{4+}). The pre-edge region is shown in the inset.

Perhaps, the clearest information is contained in the so-called pre-edge region between 7112 and 7116 eV, shown in the inset of Figure 12. Note a clear shift in the maxima of the peaks for x = 0.50 (red line) and x = 0.75 (green line) toward higher energies approaching the peak for $SrFeO_3$ (black line). This suggests a significant increase in Fe^{4+} content for x = 0.75 relative to x = 0.50, which is consistent with the Mössbauer result of Table 6. The Fe^{3+}/Fe^{4+} ratio for the x = 0.25 sample from Mössbauer, not shown in Table 6, is roughly the same as that for the x = 0.50 sample, which is consistent with the lack of a shift between these two compositions (blue line for x = 0.25). Also, the peaks for all three $BaIn_{1-x}Fe_xO_{2.5+\delta}$ air-fired samples are shifted to higher energies than the lowest peak for $LaFeO_3$ (purple line), indicating some Fe^{4+} content in all of these.

XANES is also sensitive to the local Fe environment, in particular, through the pre-edge peak (inset) which occurs well below the main edge at ~ 7125 eV. The pre-edge region is a result of 1s → 3d transitions which are quadrupolar, while 1s → 4p transitions comprise the main-edge region. XANES spectra are subject to dipolar selection rules, and the pre-edge transitions are forbidden. A coordination environment which lacks a center of symmetry leads to overlap of the 3d and 4p orbitals, which adds a dipole character to the excitation, permitting a finite pre-edge peak intensity. The presence of such a relatively intense pre-edge peak in the data of Figure 12 for all x is consistent with Fe in fourfold (tetrahedral) and/or fivefold coordination (square planar) environments as these lack a center of symmetry. These proposals can be tested by analysis of X-ray PDF and Mössbauer data that one has Fe(IV) or Fe(V) for all x.

X-ray PDF. The pair distribution function, PDF, is highly sensitive to the local structure. It is clear from the Mössbauer results that the local structure of the $BaIn_{1-x}Fe_xO_{2.5+\delta}$ samples must deviate from the average structure which permits only one Fe-site. The radial pair distribution function, $G(r)$, is derived from either X-ray or neutron diffraction data taken to very large momentum transfer, $Q = 4\pi\sin\theta/\lambda$, of order 25−30 $Å^{-1}$, followed by Fourier transform to direct space. The X-ray $G(r)$ consists of peaks at distances, r, for which bond pairs exist between atoms, A and B for example. The intensity of each $G(r)$ peak, $I(r) \sim nf_Af_B$, where n is the number of atoms at the distance r and f_A and f_B are the scattering amplitudes. A comparison of the observed $G(r)$ in the nearest neighbor range 1−5 Å to a fit based on the average $Pm\bar{3}m$ structure is highly informative regarding the local structure. Such results are seen in Figure 13. It is seen immediately that the average structure model is a poor fit, particularly near $r \sim 2$ Å, where two peaks occur in the $G(r)$, whereas only a single (In/Fe)−O peak is predicted by the $Pm\bar{3}m$ model for all x. As the fitting range is increased beyond the n.n. range, the fit to the average structure, which implies a random distribution of O^{2-} vacancies, improves dramatically, as shown in Table 7. These results indicate that the highly nonrandom vacancy distribution occurs mainly in the 1−5 Å range, and beyond that, the random distribution average structure model prevails.

In order to obtain a more detailed understanding of the evolution of the local structure with increasing x, a closer

https://dx.doi.org/10.1021/acsomega.1c00416
ACS Omega 2021, 6, 6017−6029

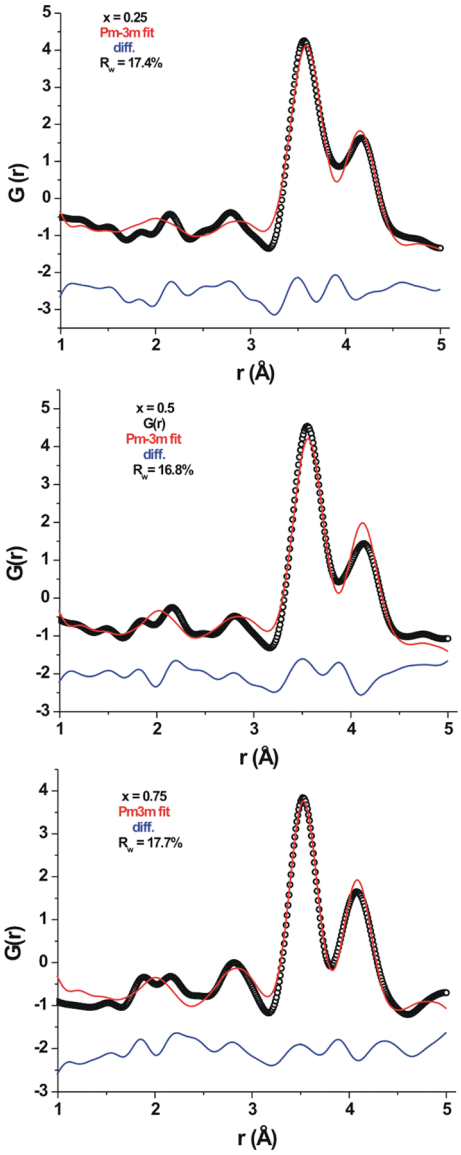

Figure 13. Comparison between the observed $G(r)$ for the air-fired samples in the range 1−5 Å with a fit based on the average $Pm\bar{3}m$ structure (top to bottom) for the air-fired samples $BaIn_{1-x}Fe_xO_{2.5+\delta}$, x = 0.25, 0.50, and 0.75.

Table 7. Results of Changing the Fitting Range for the Average $Pm\bar{3}m$ Structure for Air-Fired $BaIn_{1-x}Fe_xO_{2.5+\delta}$

x	r-range fit (Å)	Rw (%)
0.25	1−5	17.4
„	5−23	9.6
„	9−27	7.9
0.50	1−5	16.8
„	5−23	13.7
„	9−27	13.7
0.75	1−5	17.7
„	5−23	14.1
„	9−27	13.5

examination of the n.n. bonding range is warranted, as shown in Figure 14. The question to ask is, are the PDF and the two-site Mössbauer results compatible? There are clearly two broad peaks centered near ∼1.85 Å (peak 1) and ∼2.15 Å (peak 2). A likely assignment for Peak 1 is Fe^{3+}−O [CN = 4] as this agrees

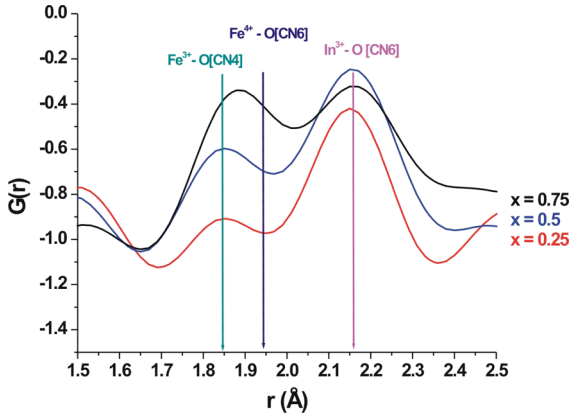

Figure 14. Evolution of $G(r)$ peaks in the n.n. region with increasing x for air-fired $BaIn_{1-x}Fe_xO_{2.5+\delta}$ compared with expected interatomic distances for Fe^{3+}−O, Fe^{4+}−O, and In^{3+}−O bonds with the indicated coordination [CN] derived both from tables of ionic radii[24] and from known distances in related materials.

with the sum of the radii. As already argued, it is highly unlikely that Fe^{4+}, either HS or LS, would prefer a tetrahedral site. Peak 2 must be In^{3+}−O[CN = 6]. Note that significant and systematic changes occur with increasing Fe content. The peaks were fitted to Gaussians, and three parameters were isolated for each peak, the position, the width, and the intensity. The fitting results are tabulated in Table 2 of the S.I. and are plotted in S.I., Figure 5. The notable result is that with the exception of the position of peak 1, all parameters increase linearly with increasing x. This is obvious from Figure 14 for the peak 1 intensity but less so for the peak 2 intensity. Why should a peak associated with In(VI)−O increase in intensity with increasing Fe content? The answer is that the peak 2 width increases with x due to contributions from Fe^{4+}−O bonds in the low r tail. For x = 0.25, there are two Fe Mössbauer sites with roughly equal fractions of Fe^{3+} and Fe^{4+}. The same is true for x = 0.50, but there is more total Fe. For x = 0.75, the Mössbauer fractions for the two sites are now inverted, with the Fe^{4+} site being dominant, >60%. The $G(r)$ position of peak 1 has shifted significantly upward and is now intermediate between the Fe^{3+}−O and Fe^{4+}−O lines, indicating the clear presence of both Fe environments. Thus, while the above-mentioned observations are only partially quantitative, it does seem possible that the PDF and results point to the same two-site model.

SUMMARY AND CONCLUSIONS

The system $BaIn_{1-x}Fe_xO_{2.5+\delta}$, x = 0.25, 0.50, and 0.75, was investigated in terms of the average and local structures and magnetic properties. Samples were prepared by air-firing and argon-firing. All materials crystallize in the defect cubic perovskite structure, $Pm\bar{3}m$, implying a random distribution of O^{2-} vacancies. From Mössbauer and XANES spectroscopies, X-ray diffraction, and PDF studies, it is clear that a mixed Fe^{3+}/Fe^{4+} valence is present in all samples to varying degrees. Attempts to prepare these phases with all Fe^{3+} were not successful. The mixed valence has profound effects on the magnetic properties. If all Fe were present as Fe^{3+}, percolation theory predicts a long-range AF order for at least the x = 0.50 and 0.75 members near or above ambient temperature. However, the air-fired x = 0.50 phase, from the a.c. susceptibility results, appears to be a nearly textbook spin glass with T_f = 5.9 K. In contrast, the magnetic ground state of the air-fired x = 0.75 phase is quite complex and

https://dx.doi.org/10.1021/acsomega.1c00416
ACS Omega 2021, 6, 6017−6029

heterogeneous. While a ZFC/FC divergence occurs below 23 K and hysteresis is observed at 2 K, the real part of the a.c. susceptibility shows no frequency dependence, ruling out the two most likely candidates, a spin glass or a superparamagnetic ground state. True magnetic Bragg peaks are not observed at 3.3 K; however, both Mössbauer and neutron diffraction data are consistent with the presence of strongly correlated magnetic clusters even at room temperature. The Mössbauer spectra show a second magnetic response which increases sharply below the ZFC/FC divergence.

Remarkably, the argon-fired samples, which have a significantly increased Fe^{3+} content, show more or less the same bulk magnetic properties with spin glass behavior for $x = 0.50$ below $T_f = 5.0$ K and a similar highly correlated ground state for $x = 0.75$ with a ZFC/FC divergence below 21 K. These ground states are attributed to competing AF and F exchange interactions involving Fe^{3+}−Fe^{3+} and Fe^{3+}−Fe^{4+}, respectively.

The local structure deviates strongly from the average $Pm\bar{3}m$ model and was investigated using ^{57}Fe Mössbauer spectroscopy, X-ray PDF, and XANES. For the air-fired samples, a two-site model involving Fe^{3+} in a fourfold site and Fe^{4+} in a sixfold or fivefold site is qualitatively consistent with all of the data. In addition, the PDF studies indicate that the local distortion from the average $Pm\bar{3}m$ model is confined to a region of ∼5 Å dimension.

The $BaIn_xFe_xO_{2.5+\delta}$ materials present two new types of magnetic ground states among the known Fe^{3+}-based $Pm\bar{3}m$ oxygen deficient perovskites, namely, a spin glass state for $x = 0.50$ and a, as of yet, poorly understood ground state for $x = 0.75$, which is clearly not either long-range ordered, a spin glass, or a superparamagnet. The closest known analogue is $SrFe_{.5}Mn_{.5}O_{2.5}$ (Sr_2FeMnO_5) which contains Fe^{3+} and Mn^{3+}, which is isoelectronic with Fe^{4+}. [6] This material also does not show a long-range order but forms finite magnetically ordered nanodomains (∼50 Å) and a rare type of superparamagnetism.

■ ASSOCIATED CONTENT

Supporting Information

The Supporting Information is available free of charge at https://pubs.acs.org/doi/10.1021/acsomega.1c00416.

Powder X-ray diffraction data, magnetic susceptibility data, neutron diffraction data, hyperfine fields derived from Mössbauer data, and analysis of X-ray PDF data (PDF)

■ AUTHOR INFORMATION

Corresponding Author

John E. Greedan − *Brockhouse Institute for Materials Research, McMaster University, Hamilton L8S 4M1, Canada; Department of Chemistry and Chemical Biology, McMaster University, Hamilton L8S 4M1, Canada;* orcid.org/0000-0003-1307-8379; Email: greedan@mcmaster.ca

Authors

Antonio D. Lozano-Gorrín − *Departamento de Química, Universidad de La Laguna, San Cristóbal de La Laguna 38200, Tenerife, Spain*

Bradley Wright − *Brockhouse Institute for Materials Research, McMaster University, Hamilton L8S 4M1, Canada*

Paul A. Dube − *Brockhouse Institute for Materials Research, McMaster University, Hamilton L8S 4M1, Canada*

Casey A. Marjerrison − *Brockhouse Institute for Materials Research, McMaster University, Hamilton L8S 4M1, Canada*

Fang Yuan − *Brockhouse Institute for Materials Research, McMaster University, Hamilton L8S 4M1, Canada*

Graham King − *Canadian Light Source, Saskatoon S7N 2V3, Canada;* orcid.org/0000-0003-1886-7254

Dominic H. Ryan − *Physics Department and Centre for the Physics of Materials, McGill University, Montreal, Quebec H3A 2T8, Canada*

Cristina Gonzalez-Silgo − *Departamento de Física, Universidad de La Laguna, San Cristóbal de La Laguna 38200, Tenerife, Spain*

○**Lachlan M. D. Cranswick** − *Canadian Neutron Beam Centre, Chalk River K0J1J0, Canada*

Andrew P. Grosvenor − *Department of Chemistry, University of Saskatchewa, Saskatoon, Saskatchewan S7N 5C9, Canada;* orcid.org/0000-0003-0024-0138

Complete contact information is available at: https://pubs.acs.org/10.1021/acsomega.1c00416

Notes

The authors declare no competing financial interest.

○Deceased.

■ ACKNOWLEDGMENTS

J.E.G. acknowledges the support of the Natural Sciences and Engineering Research Council of Canada via the Discovery Grant Program. Dr Zou Finfrock is thanked for supporting the XANES experiments carried out at the APS. Sector 20 (CLS@APS) facilities at the Advanced Photon Source are supported by the US Department of Energy—Basic Energy Sciences, and the Advanced Photon Source. The use of the Advanced Photon Source, an Office of Science User Facility operated for the U.S. Department of Energy (DOE) Office of Science by Argonne National Laboratory, was supported by the U.S. DOE under contract no. DE-AC02-06CH11357. Part of the research described in this paper was performed at the Canadian Light Source, a national research facility of the University of Saskatchewan, which is supported by the Canada Foundation for Innovation (CFI), the Natural Sciences and Engineering Research Council (NSERC), the National Research Council (NRC), the Canadian Institutes of Health Research (CIHR), the Government of Saskatchewan, and the University of Saskatchewan. DR thanks the Fonds Quebecois de la Recherche sur la Nature et les Technologies for financial support.

■ REFERENCES

(1) D'Hondt, H.; Abakumov, A. M.; Hadermann, J.; Kalyuzmaya, A. S.; Rozova, M. G.; Antipov, E. V.; van Tendeloo, G. Tetrahedral chain ordering in the $Sr_2Fe_2O_5$ brownmillerite. *Chem. Mater.* **2008**, *20*, 7188−7194.

(2) Ramezanipour, F.; Greedan, J. E.; Grosvenor, A. P.; Britten, J. F.; Cranswick, L. M. D.; Garlea, V. O. Intralayer Cation Ordering in a Brownmillerite Superstructure: Synthesis, Crystal, and Magnetic Structures of Ca2FeCoO5. *Chem. Mater.* **2010**, *22*, 6008−6020.

(3) Parsons, T. G.; D'Hondt, H.; Hadermann, J.; Hayward, M. A. Synthesis and Structural Characterization of La1−xAxMnO2.5(A = Ba, Sr, Ca) Phases: Mapping the Variants of the Brownmillerite Structure. *Chem. Mater.* **2009**, *21*, 5527−5538.

(4) Clemens, O.; Gröting, M.; Witte, R.; Perez-Mato, J. M.; Loho, C.; Berry, F. J.; Kruk, R.; Knight, K. S.; Wright, A. J.; Hahn, H.; Slater, P. R. Crystallographic and Magnetic Structure of the Perovskite-Type Compound BaFeO2.5: Unrivaled Complexity in Oxygen Vacancy Ordering. *Inorg. Chem.* **2014**, *53*, 5911−5921.

(5) Ramezanipour, F.; Greedan, J. E.; Cranswick, L. M. D.; Garlea, V. O.; Donaberger, R. L.; Siewenie, J. Systematic Study of Compositional and Synthetic Control of Vacancy and Magnetic Ordering in Oxygen-Deficient Perovskites Ca2Fe2-xMnxO5+yand CaSrFe2-xMnxO5+y (x = 1/2, 2/3, and 1; y = 0-1/2). *J. Am. Chem. Soc.* **2012**, *134*, 3215−3227.
(6) Ramezanipour, F.; Greedan, J. E.; Siewenie, J.; Proffen, T.; Ryan, D. H.; Grosvenor, A. P.; Donaberger, R. L. Local and Average Structures and Magnetic Properties of Sr2FeMnO5+y,y= 0.0, 0.5. Comparisons with Ca2FeMnO5and the Effect of the A-Site Cation. *Inorg. Chem.* **2011**, *50*, 7779−7791.
(7) Ramezanipour, F.; Greedan, J. E.; Siewenie, J.; Donaberger, R. L.; Turner, S.; Botton, G. A. A Vacancy-Disordered, Oxygen-Deficient Perovskite with Long-Range Magnetic Ordering: Local and Average Structures and Magnetic Properties of Sr2Fe1.5Cr0.5O5. *Inorg. Chem.* **2012**, *51*, 2638−2644.
(8) King, G.; Ramezanipour, F.; Llobet, A.; Greedan, J. E. Local structures of Sr2FeMnO5+y (y=0, 0.5) and Sr2Fe1.5Cr0.5O5 from reverse Monte Carlo modeling of pair distribution function data and implications for magnetic order. *J. Solid State Chem.* **2013**, *198*, 407−415.
(9) Berastegui, P.; Eriksson, S.-G.; Hull, S. A neutron diffraction study of the temperature dependence of Ca2Fe2O5. *Mater. Res. Bull.* **1999**, *34*, 303−314. Geller, S.; Grant, R. W.; Gonser, U.; Wiedersich, H.; Espinosa, G. P. On the Neel temperature of $Ca_2Fe_2O_5$. *Appl. Phys. Lett.* **1967**, *25A*, 722−723.
(10) Ramezanipour, F.; Cowie, B.; Derakhshan, S.; Greedan, J. E.; Cranswick, L. M. D. Crystal and magnetic structures of the brownmillerite compound Ca2Fe1.039(8)Mn0.962(8)O5. *J. Solid State Chem.* **2009**, *182*, 153−159.
(11) Hona, R. K.; Huq, A.; Mulmi, S.; Ramezanipour, F. Transformation of Structure, Electrical Conductivity, and Magnetism in AA′Fe2O6−δ, A = Sr, Ca and A′ = Sr. *Inorg. Chem.* **2017**, *56*, 9716−9724.
(12) Battle, P. D.; Bollen, S. K.; Gibb, T. C.; Matsuo, M. The crystal and magnetic structures of Ca2Cr0.5Fe1.5O5 at 2.1 K. *J. Solid State Chem.* **1991**, *90*, 42−46. Grenier, J. C.; Menil, F.; Pouchard, M.; Hagenmuller, P. *C. R. Acad. Sci. Paris* **1973**, *C277*, 647.
(13) Schmidt, M.; Campbell, S. J. Crystal and Magnetic Structures of Sr2Fe2O5 at Elevated Temperature. *J. Solid State Chem.* **2001**, *156*, 292−304.
(14) Gregory, D. H.; Weller, M. T. Phases in the System Ba2M2-xCuxO4+δ, M = In, Sc: Structure and Oxygen Stoichiometry. *J. Solid State Chem.* **1993**, *107*, 134−148.
(15) Fujishiro, F.; Izaki, M.; Hashimoto, T. Enhancement of the oxygen desorption/absorption property of BaFe1−x In x O3−δ by In substitution for Fe site. *J. Am. Ceram. Soc.* **2018**, *101*, 1696−1703.
(16) Toby, B. H.; von Dreele, R. B. GSAS-II: the genesis of a modern open-source all purpose crystallography software package. *J. Appl. Crystallogr.* **2013**, *46*, 544−549.
(17) Heald, S. M.; Brewe, D. L.; Stern, E. A.; Kim, K. H.; Brown, F. C.; Jiang, D. T.; Crozier, E. D.; Gordon, R. A. XAFS and micro-XAFS at the PNC-CAT beamlines. *J. Synchrotron Radiat.* **1999**, *6*, 347−349.
(18) Thompson, A.; Attwood, D.; Gullikson, E.; Howells, M.; Kim, K.-J.; Kirz, J.; Kortright, J.; Lindau, I.; Peanetta, P.; Robinson, A.; Scofield, J.; Underwood, J.; Vaughan, D.; Williams, G.; Winick, H. *X-ray Data Booklet*; Lawrence Berkeley National Laboratory, University of California: Berkeley, 2001.
(19) Ravel, B.; Newville, M. ATHENA and ARTEMIS Interactive Graphical Data Analysisusing IFEFFIT. *Phys. Scr.* **2005**, *2005*, 1007.
(20) Stinchcombe, R. B. *Dilute Magnetism in Phase Transitions and Critical Phenomena*; Domb, C., Lebowitz, J. L., Eds.; Academic Press: London, 1983; Vol. 7, p 160.
(21) Mydosh, J. A. *Spin Glasses, an Experimental Introduction*; Taylor and Francis: London, 1993; p 67.
(22) Gibb, T. C. Magnetic exchange interactions in perovskite solid solutions. Part 5. The unusual defect structure of SrFeO3 -y. *Dalton Trans.* **1985**, 1455−1470.
(23) Goodenough, J. B. *Magnetism and the Chemical Bond*; Interscience, 1963; Vol. *174*, pp 166−167.
(24) Shannon, R. D. Revised effective ionic radii and systematic studies of interatomic distances in halides and chalcogenides. *Acta Crystallogr.* **1976**, *32*, 751−767.

https://dx.doi.org/10.1021/acsomega.1c00416
ACS Omega 2021, 6, 6017−6029